

Dynamic analysis of a cylindrical boom based on Miura origami

Jianguo Cai ^{*1}, Ya Zhou ^{1a}, Xinyu Wang ^{1b}, Yixiang Xu ^{2c} and Jian Feng ^{1d}

¹ Key Laboratory of C & PC Structures of Ministry of Education,
National Prestress Engineering Research Center, Southeast University, Nanjing 210096, China
² Department of Mechanical Engineering, The University of Sheffield, Sheffield S10 2TN, United Kingdom

(Received January 24, 2018, Revised June 6, 2018, Accepted July 2, 2018)

Abstract. The dynamic behavior of the deployment and folding process of a foldable boom based on the Miura origami pattern is investigated in this paper. Firstly, mechanical behavior of a single storey during the motion is studied numerically. Then the deployment and folding of a multi-storey boom is discussed. Moreover, the influence of the geometry parameters and the number of Miura-ori elements n on the dynamic behavior of the boom is also studied. Finally, the influence of the imperfection on the dynamic behavior is investigated. The results show that the angles between the diagonal folds and horizontal folds will have great effect on the strains during the motion. A bistable configuration can be obtained by choosing proper fold angles for a given multi-storey boom. The influence of the imperfection on the folding behavior of the foldable mast is significant.

Keywords: origami; tubular structure; Miura-ori; boom; dynamic behavior; bistable

1. Introduction

Tubular structures are promising candidates for a wide range of civil and space applications (Shao 2016, Kharoob and Taman 2017, Wang *et al.* 2017). As their low volume requirements when it is used in space, it should be deployable to from foldable booms. Booms can be used to support the reflector of an antenna or form the structural framework for solar arrays and solar sails (Cadogan *et al.* 1999, Lichodziejewski *et al.* 2003).

Origami is an art of paper folding. In the past three decades, it has found a wide range of engineering applications (Filipov *et al.* 2015, Chen *et al.* 2015, Schenk *et al.* 2014, Thrall and Quaglia 2014, Kamrava *et al.* 2017). An important problem in applying origami to engineering is the rigid foldability issue. For the rigid origami, the facets and crease lines can be seen as rigid panels and hinges. In a rigid origami, all panels are not allowed to stretch or bend during the movement (Wu and You 2010). Some cylindrical deployable structures based on rigid origami patterns have been proposed by Tachi (2010). Based on the quaternion rotation sequence method and the dual quaternion method, Cai *et al.* (2016) studied the rigid foldability of the cylindrical-shaped origami patterns. Liu *et al.* (2016) presented a general kinematic model of rigid origami and proposed a family of rigidly foldable prismatic structures.

However, there are also many origami patterns for cylindrical booms, which cannot be rigidly foldable. Therefore, they require some elastic deformations of the material during the folding or deploying (Schenk 2014). But we can also use this feature by designing bistable or multi-stable cylindrical booms, which are free of stresses in two or multi configurations (You and Cole 2006, Cai *et al.* 2015a). Guest and Pellegrino (1994a, b, 1996) studied the bistable behavior of foldable thin-walled cylinders with twisted Yoshimura patterns. The geometric design of a cylindrical shell based on the Kresling pattern was studied by Cai *et al.* (2015a), and they also investigated the mechanical behavior, especially the bistable configurations of the cylinder. Kim *et al.* (2015) presented a self-deploying tubular origami, which can switches between two distinctive configurations, using this bistable behavior.

The most famous origami pattern is the Miura origami as shown in Fig. 1 (Miura 1980). Every vertex of Miura-ori has four creases, three ridge folds (solid lines in Fig. 1) and one valley fold (dashed lines in Fig. 1) or one ridge fold and three valley folds. The deployment of the Miura-ori pattern is given in Fig. 2. It can be found that the middle plane of the structure during its deployment is flat. However, for a cylinder, the system should have a curvature during the motion. Then the classical Miura-ori pattern is improved by varying the angles of the reverse folds from row to row as shown in Fig. 3 to form a curved foldable structure (Piekarski 2000). Sogame and Furuya (2000) have studied the geometrical properties of cylindrical deployable space structures, which consist of the revised Miura-ori pattern. Using detailed geometrical analysis, You and Cole (2006) pointed out that the deployment of cylinders with revised Miura-ori patterns shows strain variation within the folds. The strain peak appears during the deployment though the structure remains strain free when it is fully packaged or

*Corresponding author, Ph.D., Professor,
E-mail: j.cai@seu.edu.cn

^a Ph.D. Student, E-mail: 497667440@qq.com

^b Ph.D. Student, E-mail: iatseu@126.com

^c Senior Lecturer, E-mail: yixiang.xu@sheffield.ac.uk

^d Professor, E-mail: fengjian@seu.edu.cn

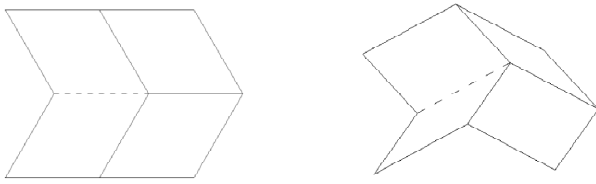


Fig. 1 Miura origami

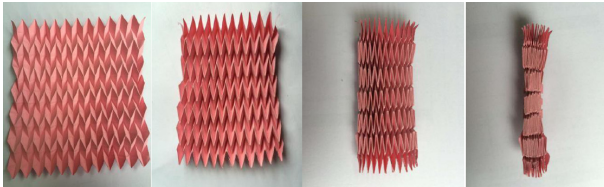


Fig. 2 Movement of Miura-ori

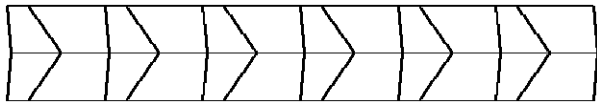


Fig. 3 Modified Miura-ori pattern

open. The geometry and deployment kinematics of a family of cylinder with reverse folds and double-reverse folds have been studied by Schenk *et al.* (2013). Senda *et al.* (2006) carried out the deployment experiments of inflatable tubes with different origami patterns. However, the link between the fold pattern and deployment characteristics was not fully understood. Cai *et al.* (2015b) have studied the geometric and mechanical behavior of a deployable cylinder with Miura origami. However, in this study, they assume that the elastic deformation can only occur in one type of elements. Then most of the elements are rigid. This condition may lead to significant errors. Moreover, the influence of the imperfection on the deployment behavior of the origami cylindrical boom has not been studied in the present literatures.

In the present paper, a dynamic analysis of a foldable cylindrical boom based on Miura origami will be carried out. Firstly, the mechanical behavior of a segment of the cylinder during the deployment will be studied. Then the effect of geometrical parameters on the dynamic behavior will be investigated. In order to obtain more insights into the deployment sequence and the corresponding material deformations, finite element simulations of multi-storey cylinder will be carried out. Finally, the influence of manufacturing imperfections will be studied.

2. Geometry design of cylinders with Miura origami

The geometry of a cylindrical boom based on the modified Miura-ori pattern as shown in Fig. 4, which is also discussed in Cai *et al.* (2015b), is studied in this section. Fig. 5(a) shows a cylinder with six storeys. The creases between the storeys are outlined by thick solid lines and

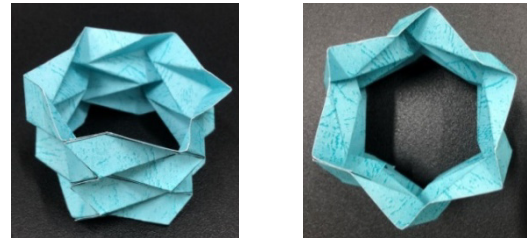


Fig. 4 Origami cylinder

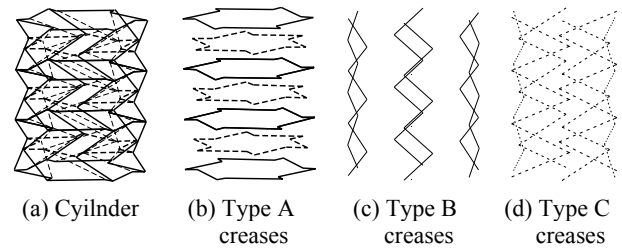


Fig. 5 Cylinder with modified Miura origami and creases

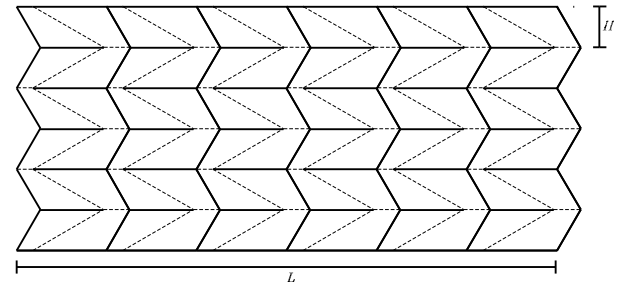


Fig. 6 Origami pattern for foldable cylinders

thick dashed lines, which are denoted by Type A creases as shown in Fig. 5(b). The adjacent storeys are symmetry of the polygon formed by Type A creases. As given in Figs. 5(c) and (d), Type B and Type C creases are diagonal bracing fold lines. In this model, Type B creases are ridge lines and Type C creases are valley lines. The origami pattern of the cylinder, as shown in Fig. 6, can be obtained by cutting along one of Type B creases. The length of this origami pattern is L and the height of half storey is H . Each half storey has $2n$ quadrilateral panels ($n = 6$ for the model shown in Fig. 6).

3. Deployment of one segment

In this section, one storey of the boom is chosen as a basic segment to study the mechanical behavior of the deployable cylinder. The cylinders are modeled as pin-jointed frameworks, where bars and pin-joints respectively represent fold lines and vertices in the crease pattern. As the basic unit of the cylinder is a quadrilateral plate, then it is important to avoid trivial internal mechanisms. In this paper, two additional bars, which are dash lines shown in Fig. 7, are added on the diagonal lines of the quadrilateral to eliminate redundant internal mechanisms. The angles between the diagonal folds and horizontal folds are defined

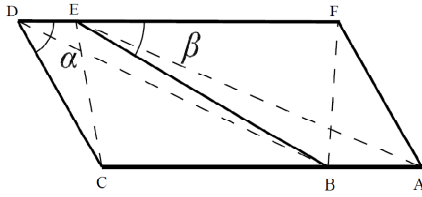


Fig. 7 Pin-jointed frameworks for the basic element of Miura-ori pattern

as α and β .

The deploying of the basic storey of the foldable boom is simulated with nonlinear finite element analysis using ABAQUS. For simplicity, truss elements are used with constitutive model defined by logarithmic strain measure. The outer vertices of the bottom polygons are constrained in the vertical and radial directions. The inner vertices of the bottom polygon are only constrained in the vertical directions. The analysis is carried out with displacement control, by defining vertical displacement at the outer vertices of the top polygons. Then for each incremented value of displacement, the axial strains of bars, external nodal loads and nodal displacements are calculated using the arc length method. The Young's modulus of the bars is $E = 2.1 \times 10^5$ MPa and the cross-section area of bars is $A = 393$ mm². In the initial fully closed configuration, the lengths of bars EF, DE, BE are given as $l_{EF} = 500$ mm, $l_{DE} = 2265.61$ mm, $l_{BE} = 2517.29$ mm. Then if the angles α , β and the number of the Miura-ori elements n are given, the lengths of other bars in the initial configuration can be obtained with a geometric method.

3.1 Influence of α and β

The results of four cases, $\alpha = 40^\circ$ and $\beta = 10^\circ$, $\alpha = 50^\circ$ and $\beta = 20^\circ$, $\alpha = 60^\circ$ and $\beta = 30^\circ$, $\alpha = 70^\circ$ and $\beta = 40^\circ$, are presented in this section. The number of Miura-ori elements n is assumed to be 6. The bar strains during the deployment are given in Fig. 8. It can be seen from this figure that the change trend of strains of these bars can be classified into two groups. Group I contains bars AB, EF, AE, BD, BF, CE, BE and Group II have bars BC, DE, CF. For the cases of $\alpha = 40^\circ$ and $\beta = 10^\circ$, $\alpha = 50^\circ$ and $\beta = 20^\circ$, $\alpha = 60^\circ$ and $\beta = 30^\circ$, the bars of Group I have a negative strain, and hence under compression and the bars of Group II have a positive strain, showing a tension. The absolute values of strains increase with the increase of the applied nodal displacements. Moreover, the absolute values of strains decrease with the increase of α and β when the systems have the same nodal displacement. For the case of $\alpha = 70^\circ$ and $\beta = 40^\circ$, the bars of Group I have a positive strain, which corresponds to a tension. The bar strains increase firstly and then descends with the increase of the applied nodal displacement. Fig. 8 also shows that the bars of AB, BC, DE, EF, CF and BE, which are corresponding to the ridge and valley lines, have higher strains than bars of AE, BD, CE and BF, which are related to the bending behavior of the quadrilateral plate.

In this numerical simulation, the nodal displacements are applied on the vertices of the polygon. In addition, for practical engineering cases, nodal loads are investigated

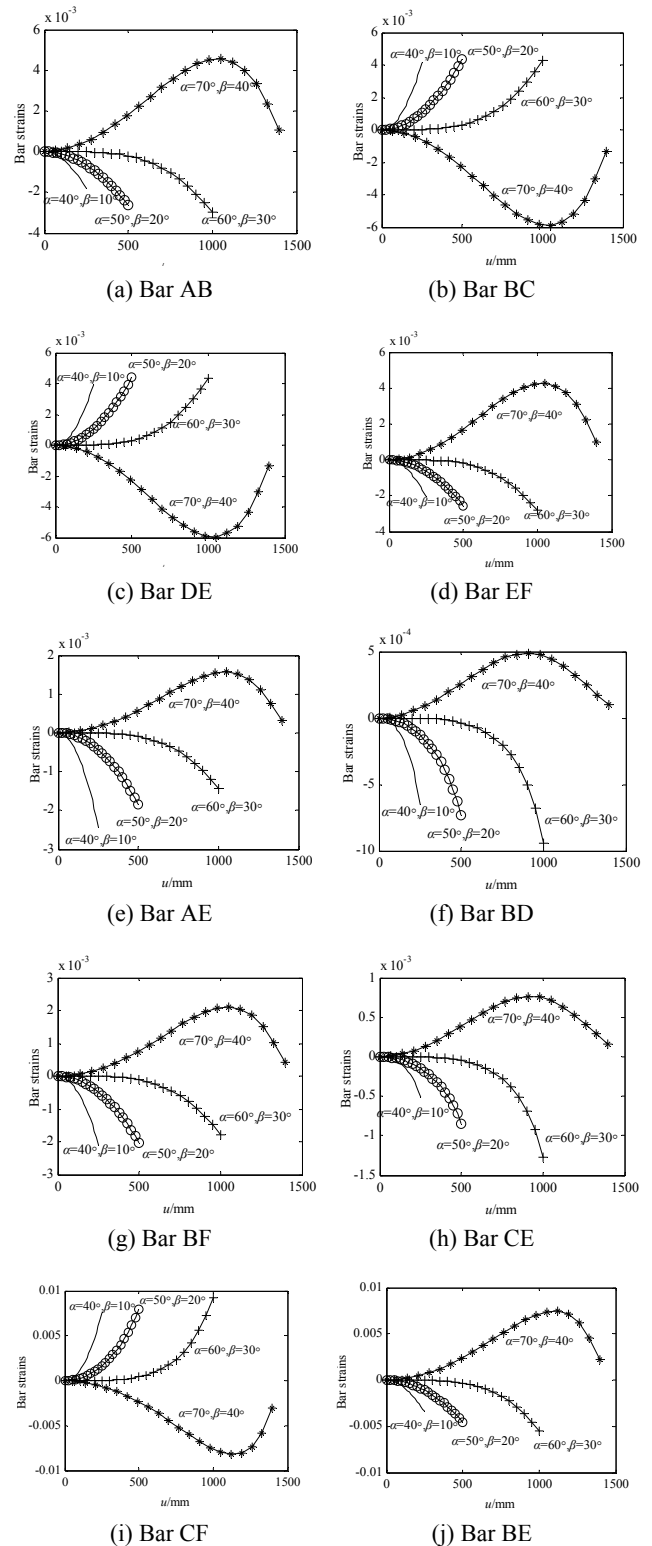


Fig. 8 Bar strains during the deployment with different angles α and β

when external nodal forces/loads are applied on these vertices. It can be seen from Fig. 9 that the deployment forces on vertices F and E have the opposite direction. For the cases of $\alpha = 40^\circ$ and $\beta = 10^\circ$, $\alpha = 50^\circ$ and $\beta = 20^\circ$, $\alpha = 60^\circ$ and $\beta = 30^\circ$, the absolute values of deployment forces increase with the increase of the applied nodal

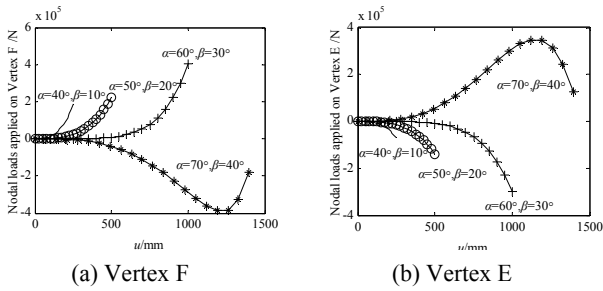


Fig. 9 Deployment forces during the deployment with different angles α and β

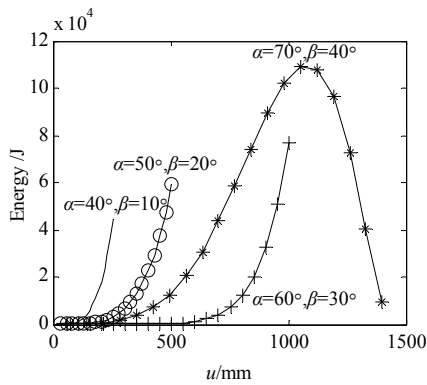


Fig. 10 Energy of the boom during the deployment with different angles α and β

displacements. For the case of $\alpha = 70^\circ$ and $\beta = 40^\circ$, the deployment forces increase firstly and then descending with the increase of the applied nodal displacement. Moreover, when the booms have the same nodal displacement, the absolute values of deployment forces decrease whilst α and β are raised. However, the absolute maximal values of deployment forces increase with the rise of α and β .

3.2 The influence of number of elements n

In order to discuss the influence of the number of elements n on the structure, four cases are studied. The numbers of elements n are assumed to be 5, 6, 8 and 9, respectively. The angle β is chosen to be 30° . Thus the corresponding angles α are $66^\circ, 60^\circ, 52.5^\circ$ and 50° . As bars AB, EF, AE, BD, BF, CE, BE behaves similarly and bars BC, DE, CF also have similar behavior, only strains of bars AB and BC during the deployment are shown in Fig. 11. For the cases of $n = 6, 8, 9$, the bar AB have a negative strain, i.e., under compression and the bar BC have a positive strain and hence in tension. The absolute values of strains increase with the rise of the applied nodal displacements. Moreover, the absolute values of strains increase with the increase of n when the booms have the same nodal displacement. For the case of $n = 5$, the bar AB firstly have a positive strain and then becomes a negative strain. The bar strains initially increases with u till it reach the maximum and then reduces to zero followed by a further decrease. This is a bistable phenomenon, which shows another zero point of the bar strain curves except for the initial stable unstressed configuration.

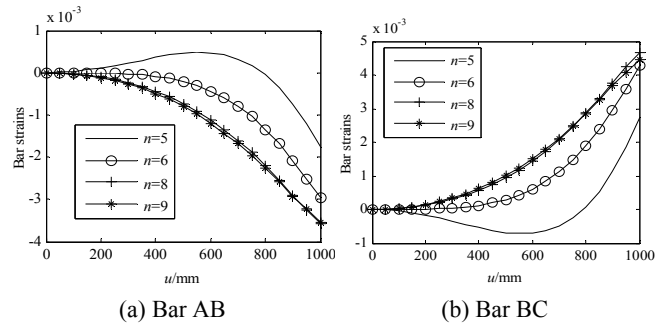


Fig. 11 Bar strains during the deployment with different n

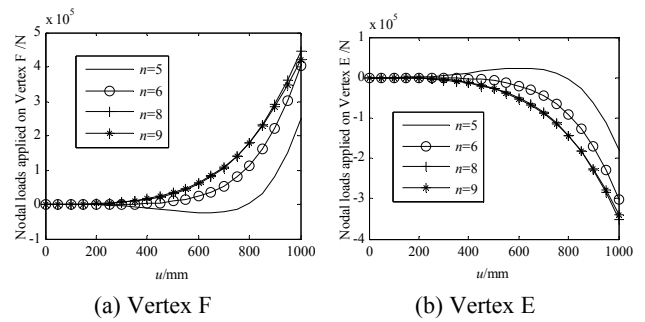


Fig. 12 Deployment forces during the deployment with different n

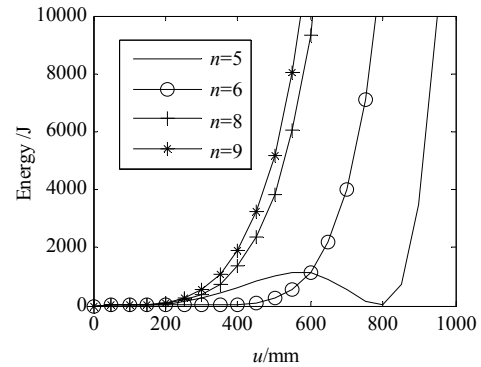


Fig. 13 Energy of the boom during the deployment with different n

The nodal loads applied on Vertices F and E during the deployment are shown in Fig. 12. It can be seen from this figure that the deployment forces on vertices F and E have the opposite direction. For the cases of $n = 6, 8, 9$, the absolute values of deployment forces increase with the increase of the applied nodal displacements. For the case of $n = 5$, the deployment forces increase firstly and then descend to zero and then change direction. Moreover, the absolute maximal values of deployment forces during the motion increase with the increase of n .

The energy variation of the basic storey of the boom during the motion with different n is shown in Fig. 13. It can be seen from this figure that the energy increases during the deployment for the cases of $n = 6, 8, 9$. However for $n = 5$, the energy goes up first and then goes down to the minimum energy point and then increase. In other words,

there are two stable configurations corresponding to the minimum energy points.

With a further study, it can be found that for a boom with $n = 4$, the energy also have two minimum points. When $n = 3$, if the angle $\beta = 30^\circ$, the corresponding angles α is then larger than 90° . Therefore, only the booms with $n = 3$ and 4, it has a bistable behavior when the $\beta = 30^\circ$.

To investigate the motion path and dynamic behavior of the multi-storey foldable booms, a four-storey boom is chosen as an example. The pin-jointed frameworks of the four-storey boom are given in Fig. 14. In order to trace the equilibrium path of the uniform motion, additional vertical restraints are added at the vertices of each horizontal polygon. The geometry of the basic element is the same as those given in Section 3.

The deployment process of the four-storey boom with $\alpha = 60^\circ$ and $\beta = 30^\circ$ is shown in Fig. 15. In the final fully deployable configuration, the height of the boom is 4000 mm and the height of every storey is 1000 mm. Therefore, the displacement applied in the top nodes of the boom is 4000 mm. The four stories of the boom following the sequence from bottom to top are defined as 1st floor to 4th floor. The vertical nodal displacements of each storey are given in Fig. 16. It can be found that the boom deploys uniformly.

Four cases, $\alpha = 40^\circ$ and $\beta = 10^\circ$, $\alpha = 50^\circ$ and $\beta = 20^\circ$, $\alpha = 60^\circ$ and $\beta = 30^\circ$, $\alpha = 70^\circ$ and $\beta = 40^\circ$, are studied in this section to investigate the influence of the geometry on the dynamic behavior of the boom. The number of Miura-ori elements n is chosen as 6. The required nodal loads applied on the top facet of the boom are given in Fig. 17. It can be found from this figure the changing trend of the boom is similar as those of the basic storey given in Section 3.

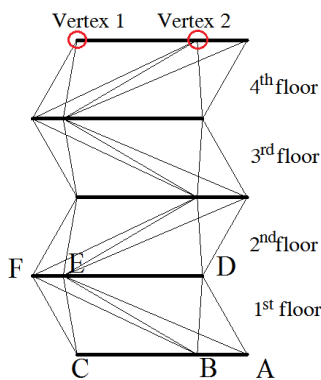


Fig. 14 Pin-jointed frameworks for the basic element of four-storey booms

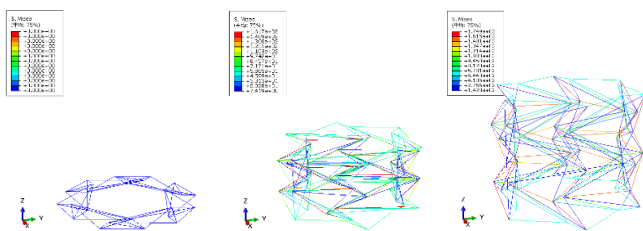


Fig. 15 The deployment process of four-storey booms

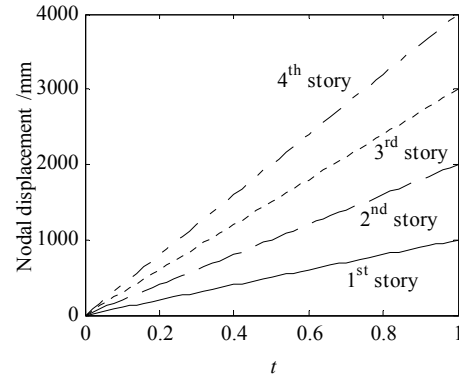


Fig. 16 Vertical nodal displacement during the deployment

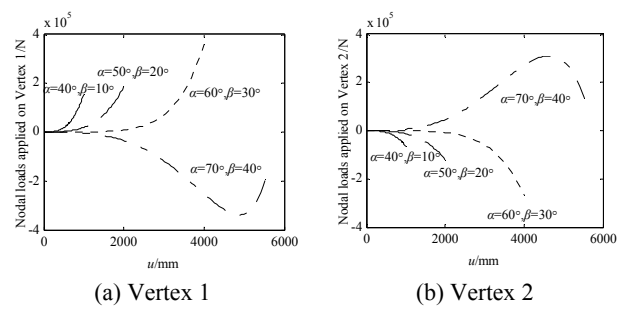


Fig. 17 Deployment forces of the boom

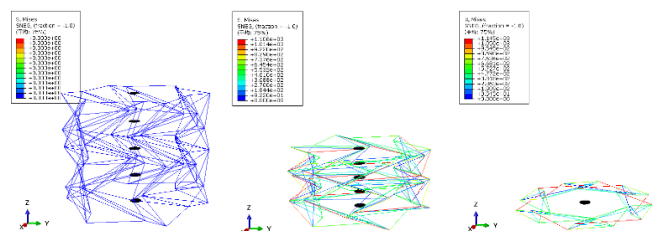


Fig. 18 The folding process of four-storey booms

The folding process of the boom when $\alpha = 60^\circ$, $\beta = 30^\circ$ and $n = 6$ is shown in the Fig. 18. In order to prevent the storey passing through each other, an additional shell is defined in the center of each polygon of every storey. The contact pairs are set between the adjacent shells. The vertical displacements of all vertices of every storey are attached to the shell. Therefore, there will be contact forces between the adjacent shells when they come into contact each other. When the two shells approach each other, the contact force increases and keep the storey from disengaging from the folded configuration.

4. Effects of imperfection

Imperfections always have great influence on the structural behavior (Ghazijahani *et al.* 2015, Li and Wu 2017). For the boom, the inaccuracy in construction and installation may have a great influence on the mechanical behavior of the structure. Guest and Pellegrino (1996)

studied the effect of misaligning the final seam of a foldable cylinder during manufacture. These errors were simulated by imposing an initial strain on the bars which cross the final join-line of the cylinder. However, this error is an imperfection of the element. In this study, a system imperfection is considered. The consistent imperfection mode method is chosen to investigate the geometrical imperfections. The imperfection distribution is assumed to be consistent with the eigenvalue buckling modes. As suggested in Cai *et al.* (2017), we have set up the first ten eigenvalue buckling modes of imperfections for foldable masts.

The initial height of the boom is 4000 mm and the height of every storey is 1000 mm. The number of Miura elements n is assumed to be 5, 6, 8 and 9, respectively. The angle β is assumed to be 30° thus giving the angles α 66° , 60° , 52.5° and 50° . The finite element model was get by modifying the joint coordinates of the initial geometry model according to the eigenvalue buckling modes. The maximal value of the imperfection assumed as one of three hundreds of the length of the boom. Therefore, the maximal value of the imperfection is 13.3 mm in this paper.

Fig. 19 shows the curve of energy versus the imposed nodal displacement of the perfect and imperfect booms during the folding when $n = 5$. Under different imperfection

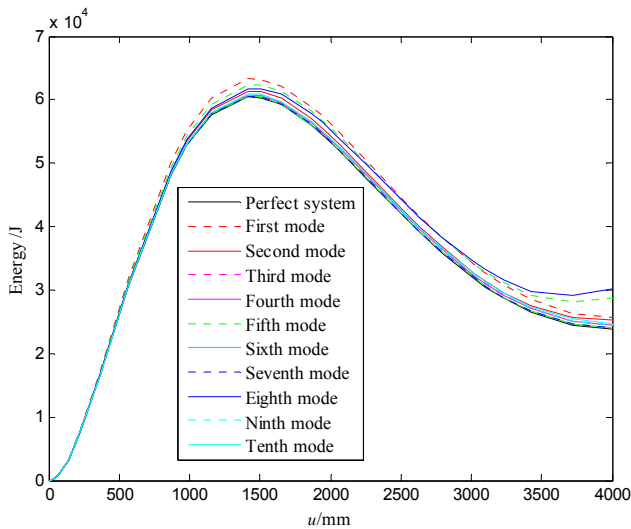
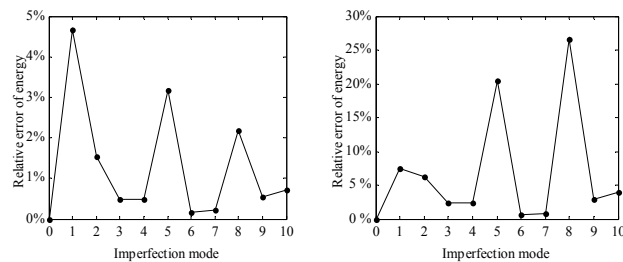


Fig. 19 Energy of perfect and imperfect booms during the folding when $n = 5$



(a) Configuration corresponding to the maximal energy

(b) Final fully deployable configuration

Fig. 20 Effects of imperfections when $n = 5$

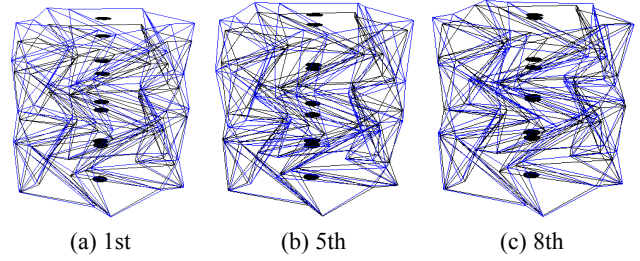


Fig. 21 Eigenvalue buckling modes when $n = 5$ (Undeformed configurations in black and deformed configurations in blue)

modes, the energy curves of the boom are almost similar. They firstly rise and then drop. They all have maximal points. The relative error of the energy during the folding of the boom is given in Fig. 20. In this figure, '0' denotes the perfect boom and '1' denotes the imperfect boom based on the first eigenvalue buckling mode. Then E_0 represents the energy of the perfect boom and E_i represents the energy of the imperfect boom based on the i^{th} eigenvalue buckling mode. The relative error of the energy is defined as $(E_i - E_0)/E_0$, which is used to measure the influence of imperfection. The relative error of the energy corresponding to the maximal energy is shown in Fig. 20(a) and the relative error of the energy in the final configuration is shown in Fig. 20(b). It can be found that the imperfections based on the 1st, 5th and 8th modes have a bigger influence on the energy of the model. These eigenvalue buckling modes when $n = 5$ are shown in Fig. 21. It can be seen from Fig. 21 that the 1st, 5th and 8th eigenvalue buckling modes deform in the z direction.

For the boom with $n = 6$, the relations between the energy of the perfect and imperfect mast and the nodal displacements are shown in Fig. 22. The relative error of the energy corresponding to the maximal energy is shown in Fig. 23(a) and the relative error of the energy in the final configuration is shown in Fig. 23(b). It can be found that the energy increases firstly and then reduces slightly.

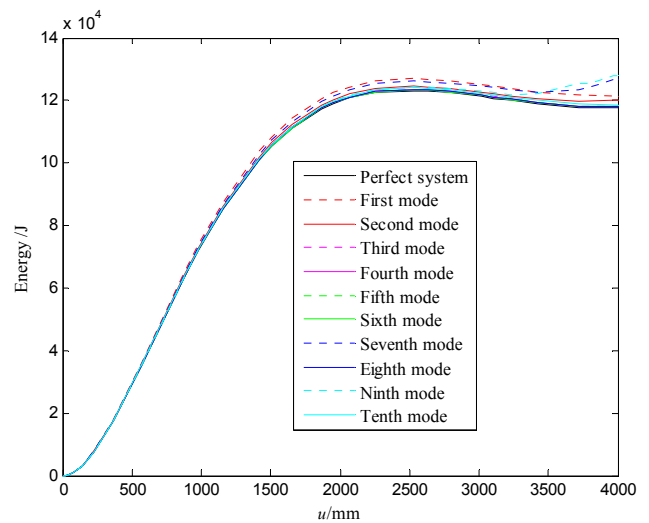


Fig. 22 Energy of perfect and imperfect booms during the folding when $n = 6$

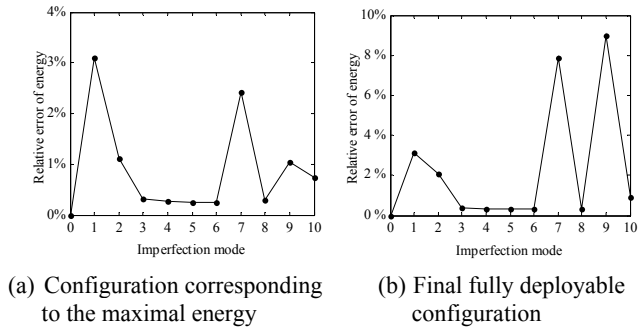


Fig. 23 Effects of imperfections when $n = 6$

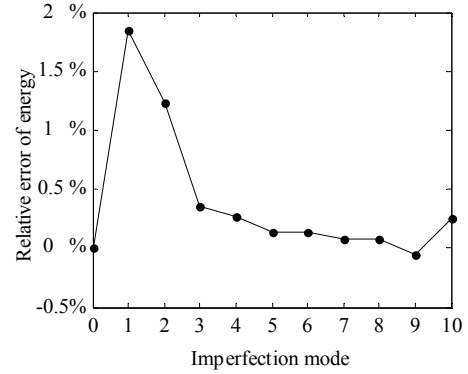


Fig. 26 Effects of imperfections when $n = 8$

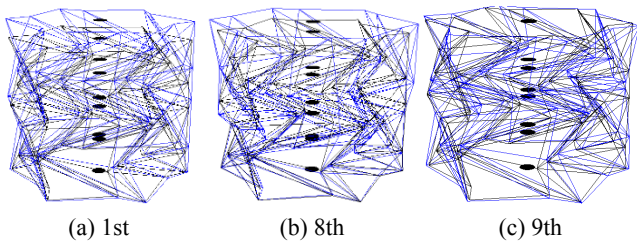


Fig. 24 Eigenvalue buckling modes when $n = 6$ (Undeformed configurations in black and deformed configurations in blue)

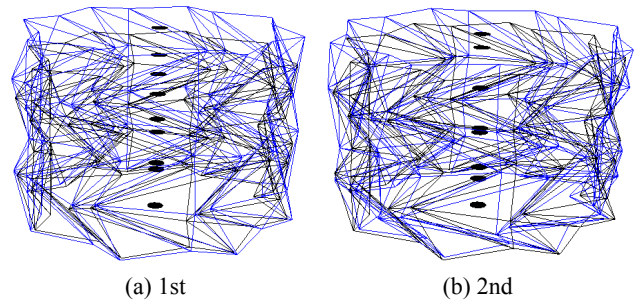


Fig. 27 Eigenvalue buckling modes when $n = 8$ (Undeformed configurations in black and deformed configurations in blue)

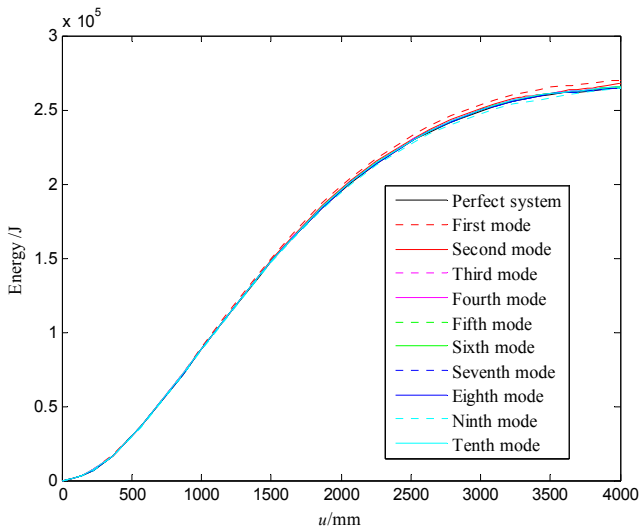


Fig. 25 Energy of perfect and imperfect booms during the folding when $n = 6$

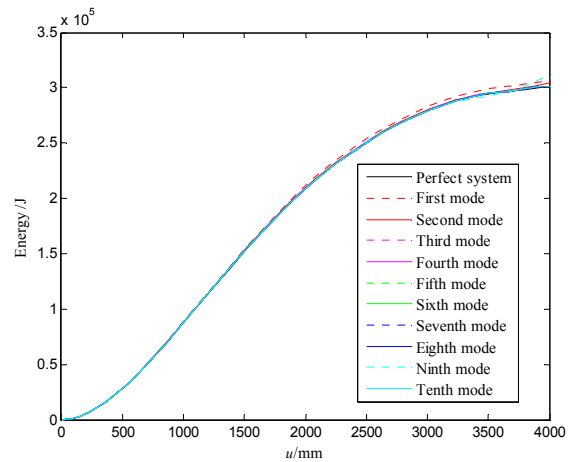


Fig. 28 Energy of perfect and imperfect booms during the folding when $n = 9$

Moreover, the energy of the boom with imperfections based on the 1st, 7th and 9th eigenvalue buckling modes are of great difference from that of the perfect mast. These eigenvalue buckling modes of the mast are given in Fig. 24. It can be seen from Fig. 24 that the 1st, 7th and 9th eigenvalue buckling modes deform in the z direction.

For the boom with $n = 8$, the relations between the energy of the perfect and imperfect boom and the nodal displacements are shown in Fig. 25. It can be found that the energy increases as the boom folds. The relative error of the energy in the final deployable configuration is shown in Fig. 26. It can be seen from this figure that the influence of

imperfection on the mechanical behavior of the boom is small except for the imperfect system based on the 1st and 2nd eigenvalue buckling modes. These two eigenvalue buckling modes of the mast are given in Fig. 27. It can be seen from Fig. 27 that the 1st and 2nd eigenvalue buckling modes deform in the z direction.

For the boom with $n = 9$, the relations between the energy of the perfect and imperfect boom and the nodal displacements are shown in Fig. 28. It can be found that the energy increases when the boom gradually folds. The relative error of the energy in the final deployable

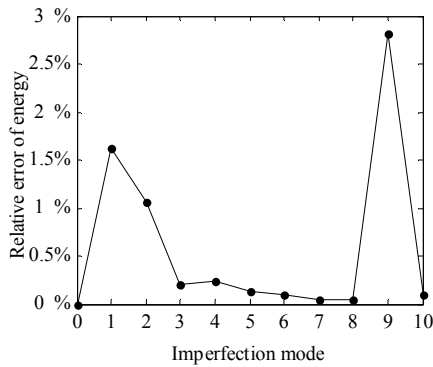


Fig. 29 Effects of imperfections when $n = 9$

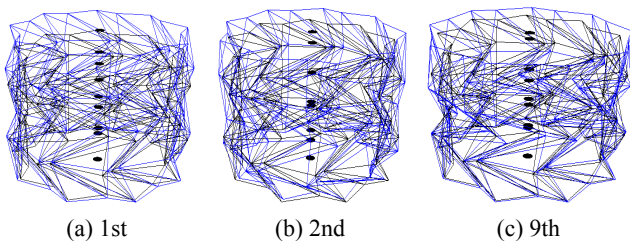


Fig. 30 Eigenvalue buckling modes when $n = 9$
(Undeformed configurations in black and deformed configurations in blue)

configuration is shown in Fig. 29. It can be seen from this figure that the influence of imperfection on the mechanical behavior of the boom is small except for the imperfect system based on the 1st, 2nd and 9th eigenvalue buckling modes. These eigenvalue buckling modes of the mast are given in Fig. 30. It can be seen from Fig. 30 that the 1st, 2nd and 9th eigenvalue buckling modes deform in the z direction.

It can be found from the previous results that when there is imperfection in the z direction, it has greater effects on the energy in the folding process of the multi-storey booms.

5. Conclusions

This paper studied the dynamic behavior of the deployment and folding process of a foldable boom based on the Miura origami pattern. Firstly, mechanical behavior of the boom during the motion is investigated by a numerical method. Moreover, the influence of the geometry parameters and the number of Miura-ori elements n on the dynamic behavior of the boom is also studied. Finally, the influence of the imperfection on the dynamic behavior is also studied. The results show that:

- For the case $n = 6$, when the angle α varies between 65° to 85° (whilst the corresponding β changes from 35° to 55°), the energy of the boom rises at first and decreases afterwards. Therefore, there exists a stable configuration during the deployment. For the case $n = 4$ and 5 , if $\beta = 30^\circ$, there will be two local minimal energy during the motion of the boom.
- The deployment of multi-storey booms is almost

uniform for all the cases studied in this paper. Therefore, the behavior of multi-storey booms is similar as the single storey boom.

- The influence of the imperfection on the folding behavior of the foldable mast is significant. The imperfection in the z direction affects the energy significantly.

Acknowledgments

The work presented in this article was supported by the National Natural Science Foundation of China (Grant No. 51578133, No. U1637207), the Natural Science Foundation of Jiangsu Province (Grant No. BK20170083), the Six top talent peak projects of Jiangsu Province (Grant No. JZ-001) and a Project Funded by the Priority Academic Program Development of Jiangsu Higher Education Institutions. Authors thank all the anonymous reviewers for their valuable comments and thoughtful suggestions which improved the quality of the presented work.

References

- Cadogan, D.P., Lin, J.K. and Grahne, M.S. (1999), "Inflatable Solar Array Technology", *Proceedings of the 37th AIAA Aerospace Sciences Meeting and Exhibit*, AIAA Paper 1999-1075.
- Cai, J.G., Deng, X.W., Zhou, Y., Feng, J. and Tu, Y.M. (2015a), "Bistable behavior of the cylindrical origami structure with Kresling pattern", *J. Mech. Des. ASME*, **137**(6), 061404.
- Cai, J.G., Deng, X.W., Feng, J. and Zhou, Y. (2015b), "Geometric design and mechanical behavior of a deployable cylinder with Miura origami", *Smart Mater. Struct.*, **24**(12), 125031.
- Cai, J.G., Jiang, C., Deng, X.W., Feng, J. and Xu, Y.X. (2015c), "Static analysis of a radially retractable hybrid grid shell in the closed position", *Steel Compos. Struct., Int. J.*, **18**(6), 1391-1404.
- Cai, J.G., Zhang, Y.T., Xu, Y.X., Zhou, Y. and Feng, J. (2016), "The foldability of cylindrical foldable structures based on rigid origami", *J. Mech. Des. ASME*, **138**(3), 031401.
- Cai, J.G., Zhang, Q., Jiang, Y.B., Xu, Y.X., Feng, J. and Deng, X.W. (2017), "Nonlinear stability analysis of a radially retractable hybrid grid shell in the closed position", *Steel Compos. Struct., Int. J.*, **24**(3), 287-296.
- Chen, Y., Peng, R. and You, Z. (2015), "Origami of thick panels", *Science*, **349**(6246), 396-400.
- Filipov, E.T., Tachi, T. and Paulino, G.H. (2015), "Origami tubes assembled into stiff, yet reconfigurable structures and metamaterials", *Proceedings of the National Academy of Sciences of the United States of America*, **112**(40), 12321-12326.
- Filipov, E.T., Liu, K., Tachi, T., Schenk, M. and Paulino, G.H. (2017), "Bar and Hinge models for Scalable Analysis of Origami", *Int. J. Solids Struct.*, **124**, 26-45.
- Ghazijahani, T.G., Jiao, H. and Holloway, D. (2015), "Experiments on locally dented conical shells under axial compression", *Steel Compos. Struct., Int. J.*, **19**(6), 1355-1367.
- Guest, S.D. and Pellegrino, S. (1994a), "The folding of triangulated cylinders, part I: geometric considerations", *J. Appl. Mech.*, **61**(4), 773-777.
- Guest, S.D. and Pellegrino, S. (1994b), "The folding of triangulated cylinders, part II: the folding process", *J. Appl. Mech.*, **61**(4), 778-783.

- Guest, S.D. and Pellegrino, S. (1996), "The folding of triangulated cylinders, part III: experiments", *J. Appl. Mech.*, **63**(1), 77-83.
- Kamrava, S., Mousanezhad, D., Ebrahimi, H., Ghosh, R. and Vaziri, A. (2017), "Origami-based cellular metamaterial with auxetic, bistable, and self-locking properties", *Scientific Reports*, 7, Article No. 46046.
- Kharoob, O.F. and Taman, M.H. (2017), "Behavior of fibre reinforced cementitious material-filled steel tubular columns", *Steel Compos. Struct., Int. J.*, **23**(4), 465-472
- Kim, J., Lee, D.Y., Kim, S.R. and Cho, K.J. (2015), "A self-deployable origami structure with locking mechanism induced by buckling effect", *Proceedings of 2015 IEEE International Conference on Robotics and Automation (ICRA)*, Seattle, WA, USA, May.
- Li, P.C. and Wu, M.E. (2017), "Stabilities of cable-stiffened cylindrical single-layer latticed shells", *Steel Compos. Struct., Int. J.*, **24**(5), 591-602
- Lichodziejewski, D., Derbès, B., West, J., Belvin, K. and Pappa, R. (2003), "Bringing an Effective Solar Sail Design Toward TRL 6", *Proceedings of the 39th AIAA/ASME/SAE/ASEE Joint Propulsion Conference and Exhibit*, AIAA Paper 2003-4659.
- Liu, S.C., Lv, W.L., Chen, Y. and Lu, G.X. (2016), "Deployable prismatic structures with rigid origami patterns", *J. Mech. Robot. ASME*, **8**, 031002.
- Miura, K. (1980), "Method of packaging and deployment of large membrane in space", *Proceedings of the 31st Congress of International Astronautical Federation*, Tokyo, Japan, pp. 1-10.
- Piekarski, M. (2000), "Constructional Solutions for Two-way-fold-deployable Space Trusses", *Proceedings of IUTAM-IASS Symposium on Deployable Structures: Theory and Applications*, pp. 301-310.
- Schenk, M., Kerr, S., Smyth, A.M. and Guest, S.D. (2013), "Inflatable cylinders for deployable space structures", *Proceedings of the First Conference Transformables 2013*, Seville, Spain, September.
- Schenk, M., Viquerat, A.D., Seffen, K.A. and Guest, S.D. (2014), "Review of Inflatable Booms for Deployable Space Structures: Packing and Rigidisation", *J. Spacecraft Rockets*, **51**(3), 762-778.
- Senda, K., Oda, T., Ohta, S., Igaras, Y., Watanabe, A., Hori, T., Ito, H., Tsunoda, H. and Watanabe, K. (2006), "Deploy Experiment of Inflatable Tube Using Work Hardening", *Proceedings of the 47th AIAA/ASME/ASCE/AHS/ASC Structures, Structural Dynamics, and Materials Conference*, AIAA Paper 2006-1808.
- Shao, Y.B. (2016), "Static strength of collar-plate reinforced tubular T-joints under axial loading", *Steel Compos. Struct., Int. J.*, **21**(2), 323-342
- Sogame, A. and Furuya, H. (2000), "Conceptual Study on Cylindrical Deployable Space Structures", *Proceedings of the IUTAM-IASS Symposium on Deployable Structures: Theory and Applications*, (Edited by S. Pellegrino and S.D. Guest), Kluwer Academic, Dordrecht, The Netherlands, September, pp. 383-392.
- Tachi, T. (2010), "Geometric considerations for the design of rigid origami structures", *Proceedings of the International Association for Shell and Spatial Structures (IASS) Symposium 2010*, Shanghai, China.
- Thrall, A.P. and Quaglia, C.P. (2014), "Accordion shelters: a historical review of origami-like deployable shelters developed by the US military", *Eng. Struct.*, **59**, 686-692.
- Wang, Y.M., Shao, Y.D. and Cao, Y.F. (2017), "Static behavior of steel tubular structures considering local joint flexibility", *Steel Compos. Struct., Int. J.*, **24**(4), 425-439
- Wu, W.N. and You, Z. (2010), "Modelling rigid origami with quaternions and dual quaternions", *Proceedings of the Royal Society A: Mathematical, Physical and Engineering Sciences*, **466**, 2155-2174.
- You, Z. and Cole, N. (2006), "Self-Locking Bi-Stable Deployable Booms", *Proceedings of the 47th AIAA/ASME/ASCE/AHS/ASC Structures, Structural Dynamics, and Materials Conference*, AIAA Paper 2006-1685.

CC